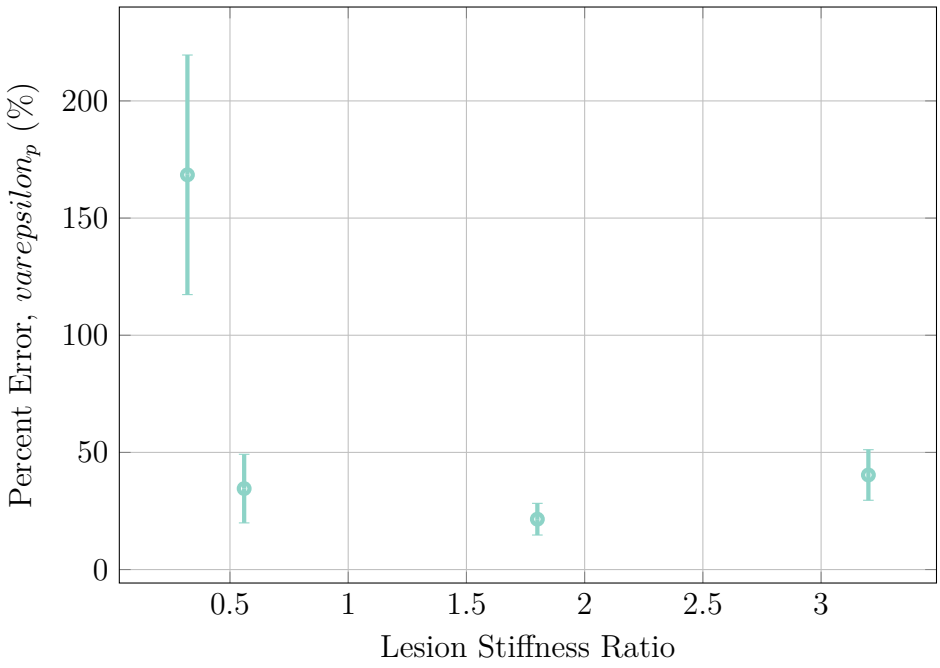

Fig. 3.6: Detection ability as it is related to true lesion stiffness ratio. For all but small lesion stiffness ratios (very unstiff lesions), results are linear and predictable. For small lesion stiffness ratios (0.32), the lesion becomes severely misrepresented. This is likely due to the algorithm "losing track" of scattering centres for the relatively large displacements induced in the significantly less stiff tissue.

$$\varepsilon_p = \left| \frac{Y_i - \hat{Y}_i}{\hat{Y}_i} \right| \times 100\,\% \tag{3.6}$$

In order to broadly investigate the critical parameter-values of the investigated models, each parameter was normalized to its investigated range and the error resulting over these ranges is given in Figs. 3.7 and 3.8.

In Fig. 3.7, it is clear to see that the most sensitive error-inducing situations occur when either the lesion is very small or if large strains are used to deform the tissue. Similarly, it is expected that if the lesion depth were increased much further, significant errors would arise with increasing depth. Logically, this may be explained due to the decreasing magnitude of displacement with increasing depth—at a certain point, the magnitude of displacement

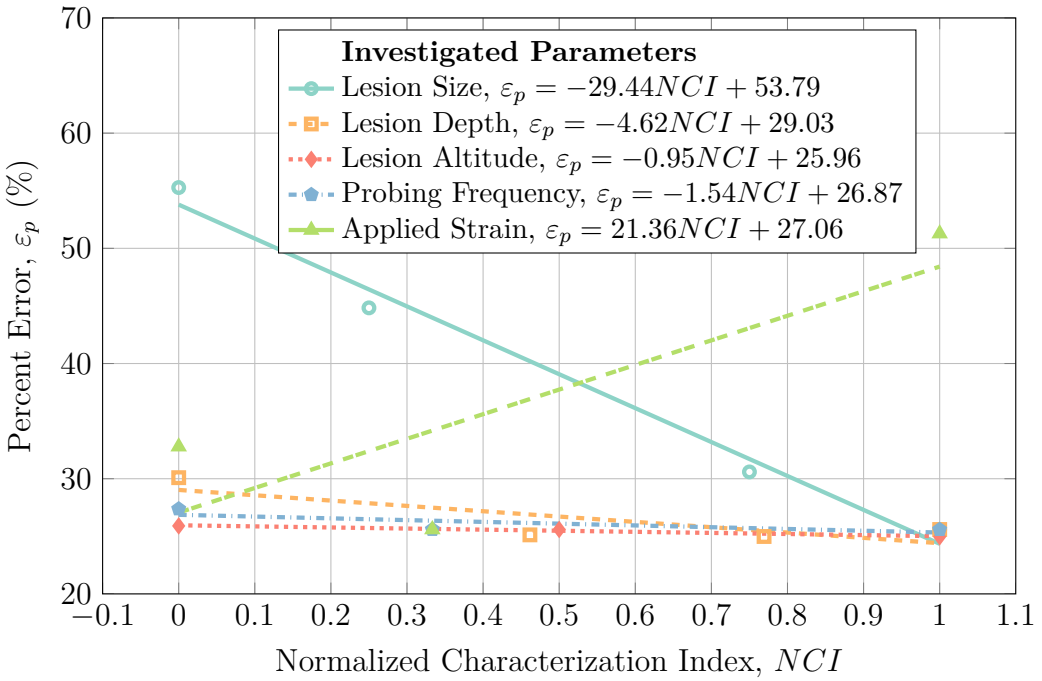

Fig. 3.7: Error characterization for range of studied parameters for the simple model of a spherical lesion embedded within soft tissue as seen in Fig. 3.1a. Each parameter has been normalized to the range studied so overly-sensitive regions may be readily distinguished. Lines represent linear regressions of the data points.

of scattering centres will be on par with the measurement noise, and the lesion will cease to be detectable.

From Fig. 3.8 it can be seen that small lesions in the Visible Human-MRI model as well as co-located lesions with large separation distances produce greater measurement errors. Conversely, lesion depth in the Visible Human-MRI model; lesion density and individual lesion size in the clustered lesion model; and boundary blur radius in the blurred-edges model do not seem to affect the measurement error significantly. Of note is the relatively large amount of static error present in the boundary blur radius model which is hypothesized to be due to lesser mean tissue stiffness in the investigated region than expected.

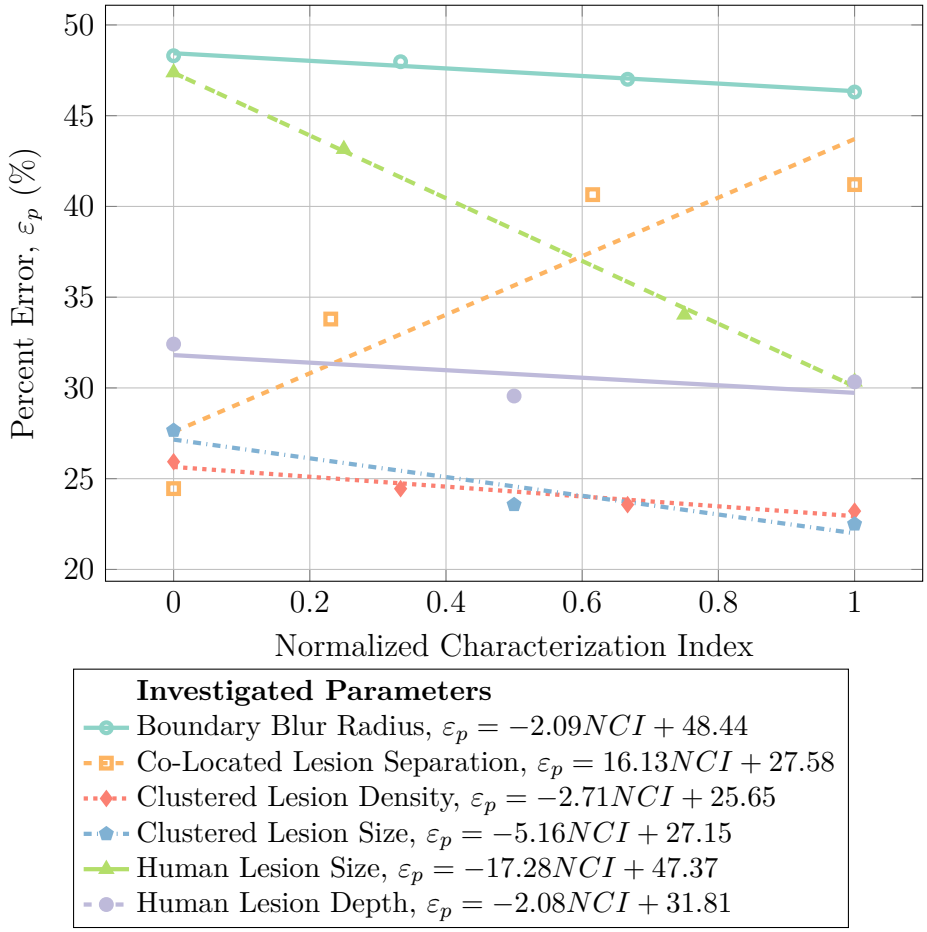

Fig. 3.8: Error characterization for range of studied parameters for the co-located lesions, blurred boundary lesions, clustered lesions, and visible human lesion models as seen in Figs. 3.1b – 3.1e. Each parameter has been normalized to the range studied so overly-sensitive regions may be readily distinguished. Lines represent linear regressions of the data.

Fig. 3.9 shows the relationship between lesion size and detection sensitivity for lesions at a depth of 10 cm in a model depth of 12.5 cm interrogated at 4 MHz with 5 % applied strain. Specifically, Fig. 3.9 shows the decreasing detection sensitivity with decreasing lesion size with the best detection sensitivity being with the largest investigated lesions with a diameter of 2.5 cm. On the opposite end, the detection sensitivity of lesions at or below 0.5 cm in diameter is questionable. Although data is lacking on the true size of forma-

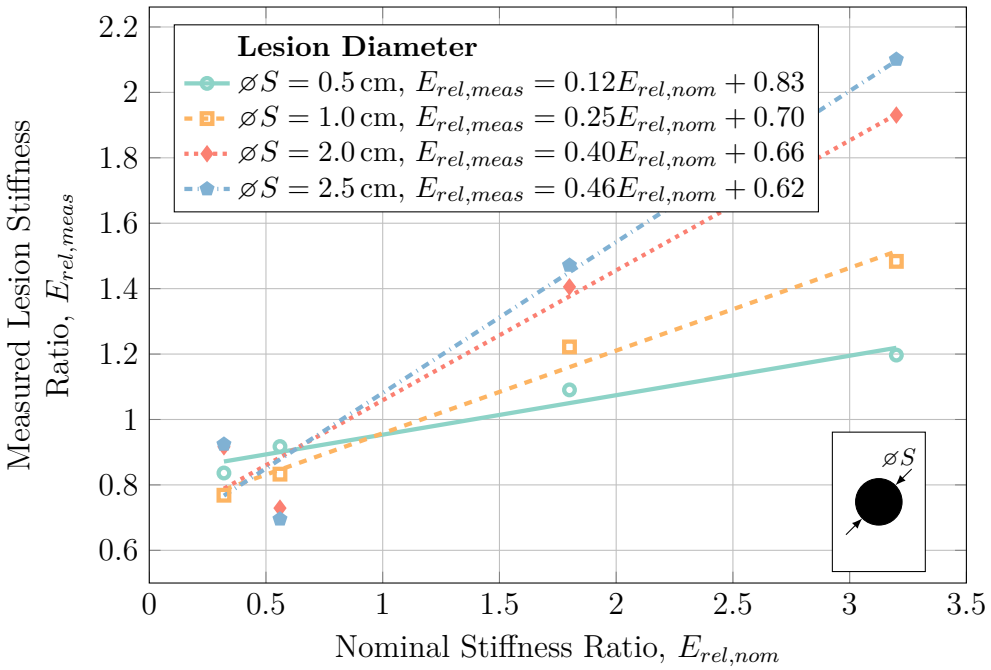

Fig. 3.9: Lesion size characterization at a depth of 10 cm with a 4 MHz ultrasound probing frequency showing increasing detection sensitivity of the lesion with increasing lesion size. Detection sensitivity is less than ideal for all cases, with the best case being for lesions approximately 2.5 cm in diameter. Lines represent linear regressions to the data.

tive DTI, MRI results indicate that untreated DTI are on the scale of multiple centimetres [67]. Thus, the ability to detect lesions of at least 1 cm in diameter should prove to be adequate to both detect and monitor DTI.

In order to investigate the effect of lesion depth on the detection sensitivity, measured strain ratios for circular lesions with a diameter of 2.5 cm located at various depths were interrogated with a 4 MHz probing frequency, and strained by 5 %. The results of this investigation are seen in Fig. 3.10.

In Fig. 3.10, it can be seen that there was little interplay between detection sensitivity and measured strain ratios at the various depths examined for all but the case of very unstiff (unstiff) lesions (with a stiffness ratio of 0.32). At such low stiffness ratios, the excessive tissue deformation interrupts the

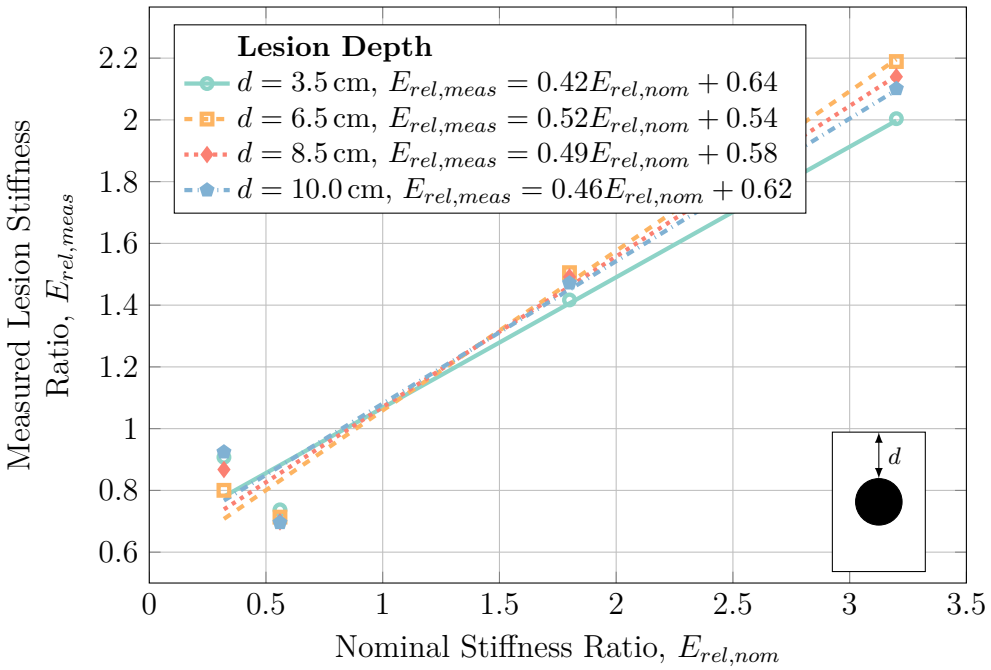

Fig. 3.10: Lesion depth characterization at a lesion diameter of 2.5 cm with a 4 MHz ultrasound probing frequency generally showing general independence of detection sensitivity on lesion depth in the tissue. Lines represent linear regressions of the data.

tissue strain estimation algorithm's ability to adequately track the induced displacements in the lesion.

Since the strain field caused by compressive forces near an extremely rigid structure embedded within a relatively unstiff domain will be significantly heterogeneous, the effect of lesion altitude above the underlying stiff bone was examined with the hypothesis that if the lesion were too close to the hard bone, it would be masked by the strain field caused by the bone's existence. A 2.5 cm diameter lesion was interrogated with a 4 MHz probing frequency and 5 % applied strain. The results of this characterization are given in Fig. 3.11.

In Fig. 3.11, it can be seen that the lesion altitude above the underlying bone had very little effect on the detection sensitivity. Although larger strain fields may be generated near the bone, it is hypothesized that the larger fields

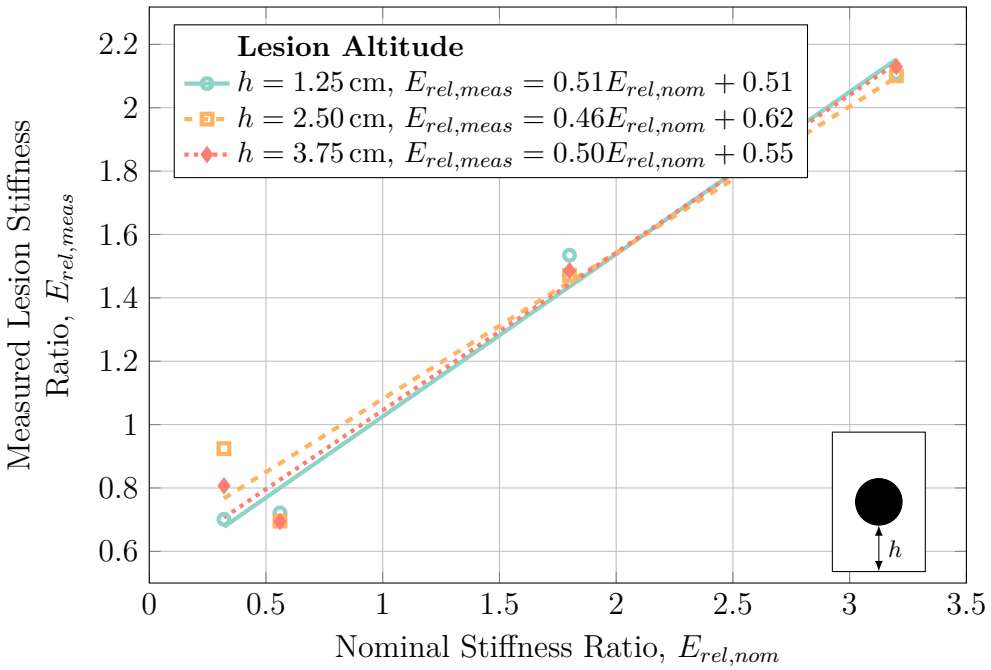

Fig. 3.11: Effect of lesion altitude above the underlying bone. Aside from erroneous results at very low lesion stiffness ratios, the effect is negligible. Lines represent linear regressions of the data.

also extend larger and so affect healthy tissue to more or less the same degree as the forming lesion.

In order to characterize the effect of using alternate ultrasound probing frequencies, simulations were carried out on lesions using probing frequencies of 2 MHz, 4 MHz, and 8 MHz. The simulated lesions had a diameter of 2.5 cm, were located at a depth of 10 cm and were strained at 5 %. The results of this study are given in Fig. 3.12.

As can be seen from Fig. 3.12, there is very little effect on the detection sensitivity from the ultrasound probing frequency that was used, therefore an appropriate frequency should be chosen so as to reach the the full depth of the bone-muscle interface at suspected DTI locations while retaining the best image resolution.

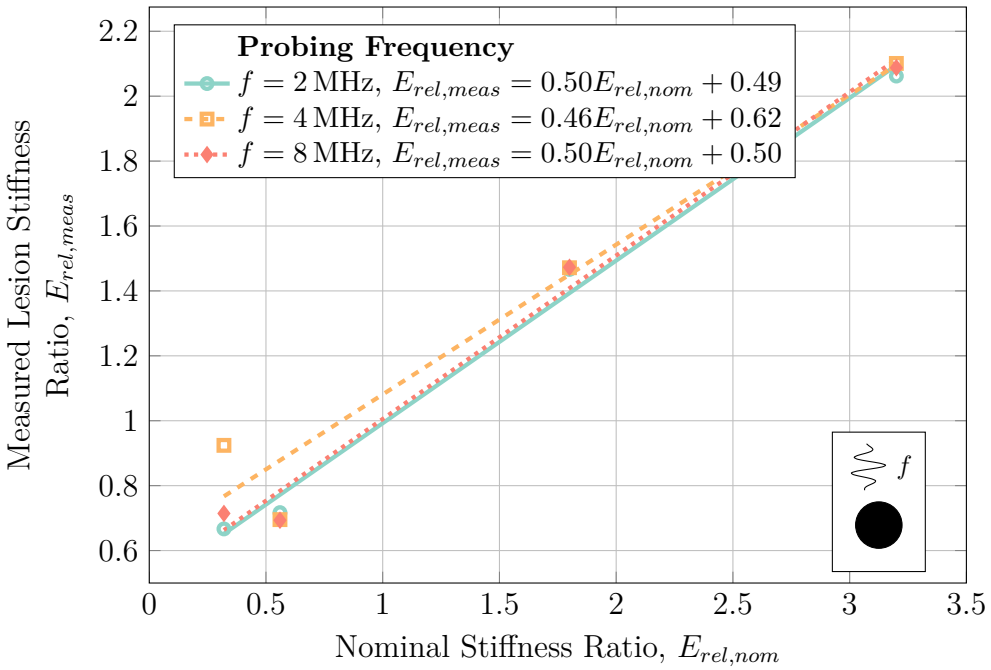

Fig. 3.12: Characterization of ultrasonic probing frequency on detection sensitivity. Apart from the requirement of using an ultrasonic frequency low enough to interrogate the desired tissue, probing frequency has negligible effect on the detection sensitivity. Lines represent linear regressions of the data.

As quasi-static ultrasound elastography is most likely to be performed via manual indentation where the exact magnitude of applied deformation is unknown, it is important to study the effect of applied strain magnitude on the detection sensitivity. Applied strains of 2.5 %, 5.0 %, and 10 % were investigated on a 2.5 cm diameter lesion at a depth of 10 cm using a probing frequency of 4 MHz; the results are given in Fig. 3.13.

While Fig. 3.13 shows a relatively constant detection sensitivity for compressive strains of 2.5 % and 5 %, compressive strains of 10 % generate significant measurement error for both very unstiff and very stiff lesions. Under large compressive strains, the tissue (either in the lesion as in the unstiff lesion case, or the surrounding tissue as in the stiff lesion case) deforms considerably which again interferes with the algorithm's ability to properly track the dis-

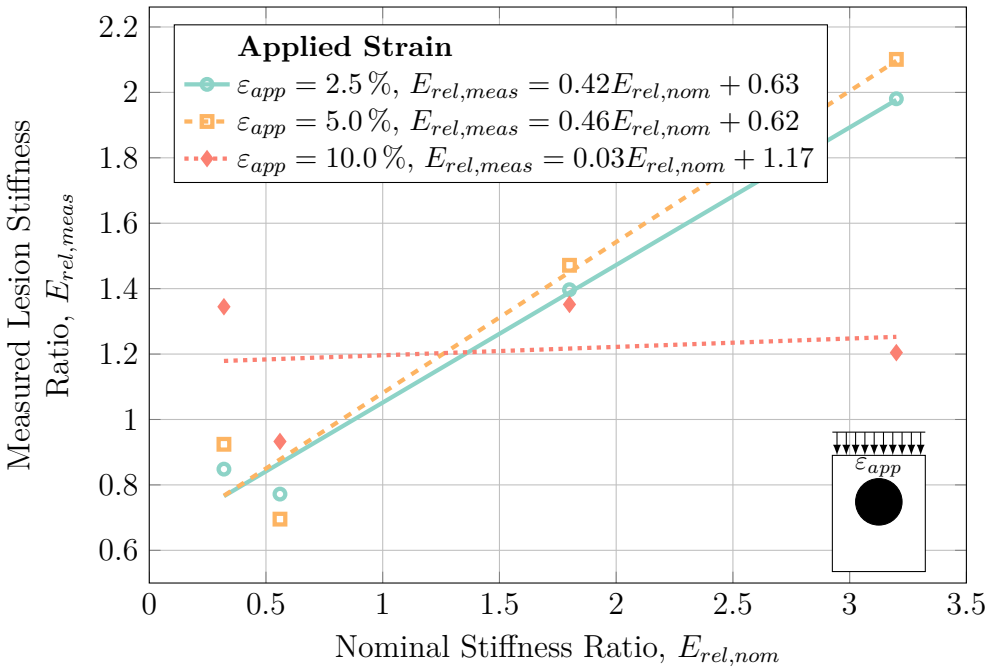

Fig. 3.13: Applied strain characterization plot for lesions with a diamater of 2.5 cm located at a depth of 10 cm interrogated at 4 MHz. There is little difference between 2.5 % and 5.0 % applied strain, while large-magnitude strains of 10 % generate significant error for both very unstiff and very stiff lesions. Lines represent linear regressions of the data.

placement of tissue. It should also be noted that applying overly large strains to an already forming deep tissue injury may cause additional unwarranted damage. Thus it is imperative that applied surface indentation be kept to reasonable bounds (2.5 % – 5 %, or 0.25 cm – 0.50 cm in 10 cm deep domains), not only for safety of the tissue but also for clarity of the diagnostic test.

To study the effect that closely spaced lesions will have on the detection sensitivity as well as how discernible the lesions will be from each other, the separation distance between two 1.0 cm diameter co-located lesions at a depth of 10 cm was examined using a 4 MHz probing frequency with 5 % applied strain magnitude. The results of this study are shown in 3.14.

While Fig. 3.14 shows that the separation distance between co-located

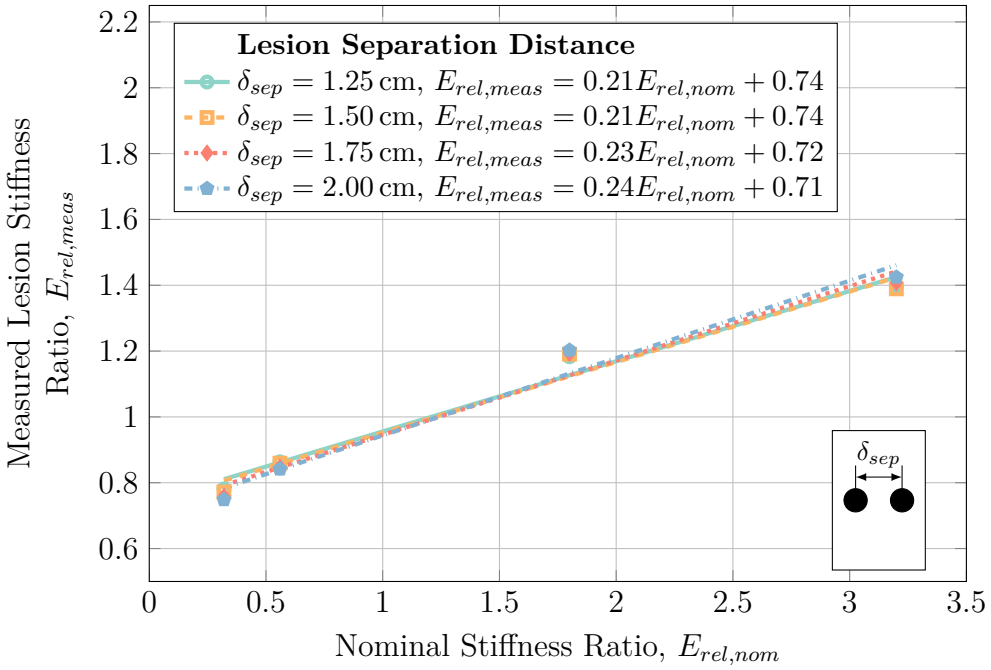

Fig. 3.14: Effect of lesion separation distance on two 1.0 cm diameter lesions co-located at a depth of 10 cm interrogated with a 4 MHz probe with 5 % applied strain. There is no negligible difference between separation distances on the detection sensitivity. Lines represent linear regressions of the data.

lesions causes a negligible effect on the detection sensitivity, Fig. 3.15 shows regions of decreased strain above and below the centreline of the lesions. While these regions had the same basal stiffness as the bulk tissue, the decreased strain pattern may obfuscate the true results by introducing "phantom lesions" which are not actually present but merely the result of the existing lesions.

While the simulations performed thus far assumed that lesions were perfect spheres with hard boundaries in order to isolate specific parameters of interest, this assumption may not always be accurate. Rather, due to the nature of injury formation, lesions may form gradual boundaries that "fade" from stiff or necrotic tissue to healthy tissue. To investigate the effect of this phenomenon on the detection sensitivity, lesions with "blurred boundaries" were investigated. Hard spherical lesions were blurred by convolving the lesion domain

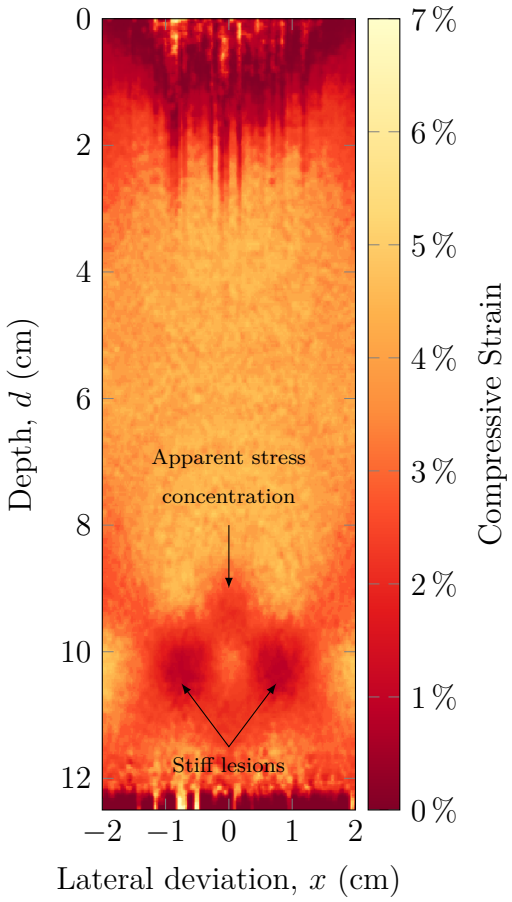

Fig. 3.15: Elastogram for two co-located lesions of 1.0 cm diameter at a depth of 10 cm interrogated using a 4 MHz probing frequency with 5 % applied strain. A pattern of decreased strain is present above and below the centerline between the two lesions while the lesions themselves are not affected by each other.

with a disc blurring kernel of varying radius. The results for this investigation on lesions with a diameter of 2.5 cm, at a depth of 10 cm and interrogated with a 4 MHz probing frequency with 5 % applied strain are given in Fig. 3.16.

Fig. 3.16 shows that there is relatively little dependence of the lesion detection sensitivity on the lesion blur radius. No matter the blur radius, quasi-static elastography substantially overestimated the stiffness of stiff lesions and underestimated the stiffness of unstiff lesions. This technique was unable to discern differences in lesion stiffness due to blur radius for the least

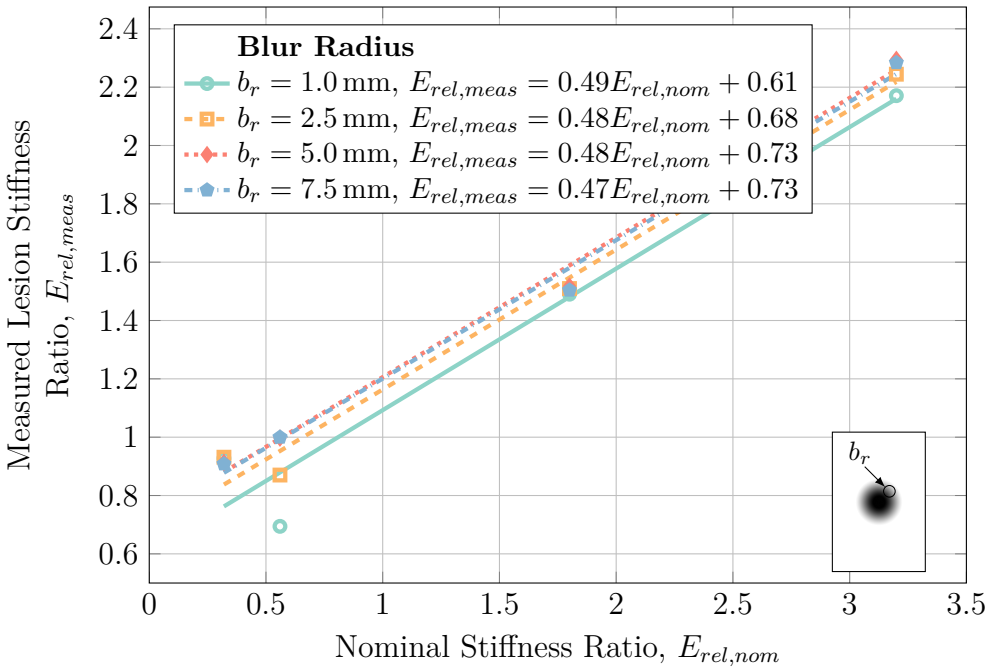

Fig. 3.16: Characterization of the effect of lesion blur radius on lesion detection sensitivity for a 2.5 cm diameter lesion at a depth of 10 cm using a probing frequency of 4 MHz and applied strain of 5 %. While there is negligible effect of the blur radius on stiff lesions, the strain ratio for unstiff lesions is considerably over-estimated. Lines represent linear regressions of the data.

stiff lesions—lesions with a nominal stiffness ratio of 0.32. Further, quasi-static elastography was generally unable to detect unstiff lesions ($E_{rel,nom} \leq 1$) whatsoever.

Similar to how lesions may have "blurred boundaries" rather that hard ones, so too may lesion composition not be homogeneous. In order to study the effect of heterogeneous regions of injured tissue, the detection sensitivity of a set of numerous small lesions located within close proximity to each other so as to form a large, heterogeneous area of diseased tissue was examined. Fig. 3.17 shows the results for this model for varying numbers of 2 mm diameter lesions in a 2.5 cm diameter circle located at a depth of 10 cm with a probing frequency of 4 MHz and 5 % applied strain. Fig. 3.19 further explores this

model by investigating the case where there are 30 small lesions per square cm with individual lesions ranging in diameter from 0.5 mm to 1.5 mm.

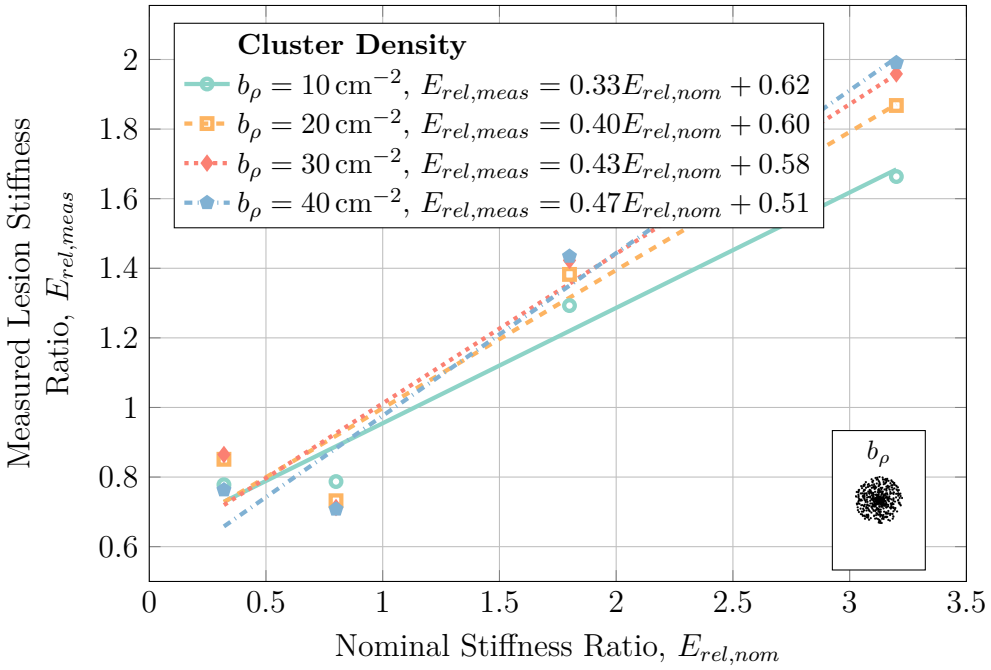

Fig. 3.17: Characterization of lesion density for a group of numerous smaller 2 mm diameter lesions comprising a large area with a diameter of 2.5 cm at a depth of 10 cm interrogated with a 4 MHz probing frequency and 5 % applied strain. Detection sensitivity decreases with decreasing lesion density, as expected. Lines represent linear regressions of the data.

The characterization plot in Fig. 3.17 for small lesion density is less linear than previous characterization plots, with lesion density having a significant effect on the detection sensitivity. Specifically, for low lesion densities, the detection sensitivity is much lower than for high lesion densities. However, this observation is warranted after examination of the elastogram produced from these results, given in Fig. 3.18, which shows how the small lesions are not individually detected but rather the entire region is detected as one large lesion. Since the average stiffness ratio over this region is less than the stiffness ratio of individual lesions, it makes sense that the "measured" strain ratio will

be less than expected.

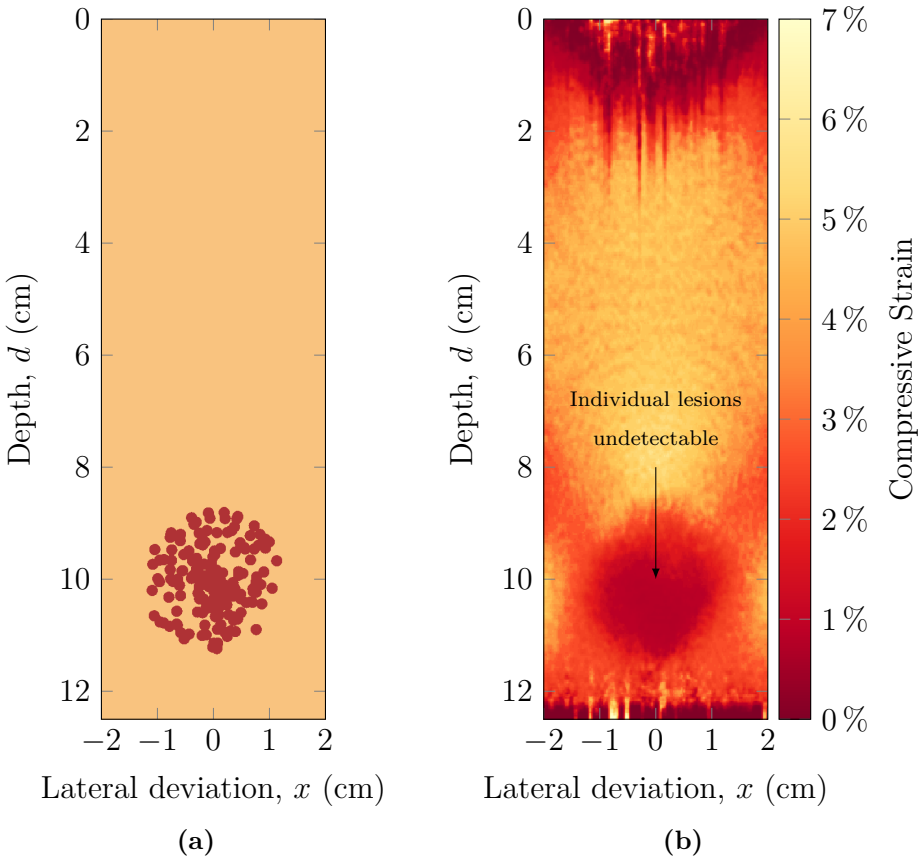

Fig. 3.18: Stiffness map (a) and corresponding elastogram (b) for a group a small lesions with a density of 10 lesions per cm^2 grouped in a 2.5 cm diameter circle at a depth of 10 cm interrogated with a 4 MHz probing frequency and 5 % applied strain. In (a), white regions are regular tissue while black regions are the small lesions. In the elastogram, individual lesions do not stand out, rather the entire region of lesions appears as one large region of unhealthy tissue.

Similar to the results shown in Fig. 3.17, changing the size of the individual small lesions does have an effect on the measured strain as seen in Fig. 3.19. In this case, when individual lesions are small, the total area occupied by lesions is lesser which results in a lesser average tissue stiffness over the grouped lesion region.

Note that although the elastography algorithm was able to detect the larger

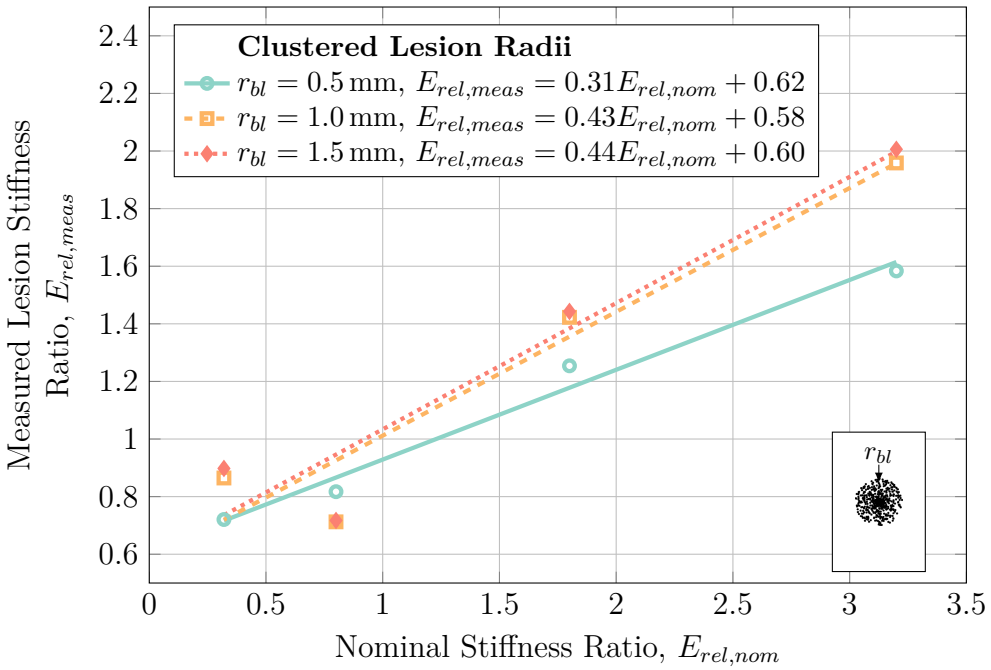

Fig. 3.19: Characterization of lesion radius for a group of numerous smaller lesions with a density of 30 lesions per cm^2 comprising a large area with a diameter of 2.5 cm at a depth of 10 cm interrogated with a 4 MHz probing frequency and 5 % applied strain. Detection sensitivity decreases with decreasing individual lesion size, as expected. Lines represent linear regressions of the data.

lesion-filled regions in these simulations, it was completely unable to discern the individual lesions comprising those regions. This is not surprising due to both the generated strain fields in the healthy tissue throughout the larger lesion area as well as the results presented in Fig. 3.9 showing poor detection sensitivity for lesions with diameters $\leq$ 1 cm while the individual lesions in this simulation had diameters of the scale of 0.5 mm – 1.5 mm.

Finally, in order to place these results within the context of a real scenario in humans, a more complicated model utilizing an MRI-acquired lesion and slides from the Visible Human Project [126] was developed. Specifically, lesion geometry was taken from a real deep tissue injury in a pig model imaged using T_2^*-weighted MRI. The human geometry was taken from a transverse

plane slice across the left ischial tuberosity such that the lesion was placed immediately superficial to the boney prominence. For this model, the overall lesion width and lesion depth were examined with results shown in Figs. 3.20 and 3.22 respectively.

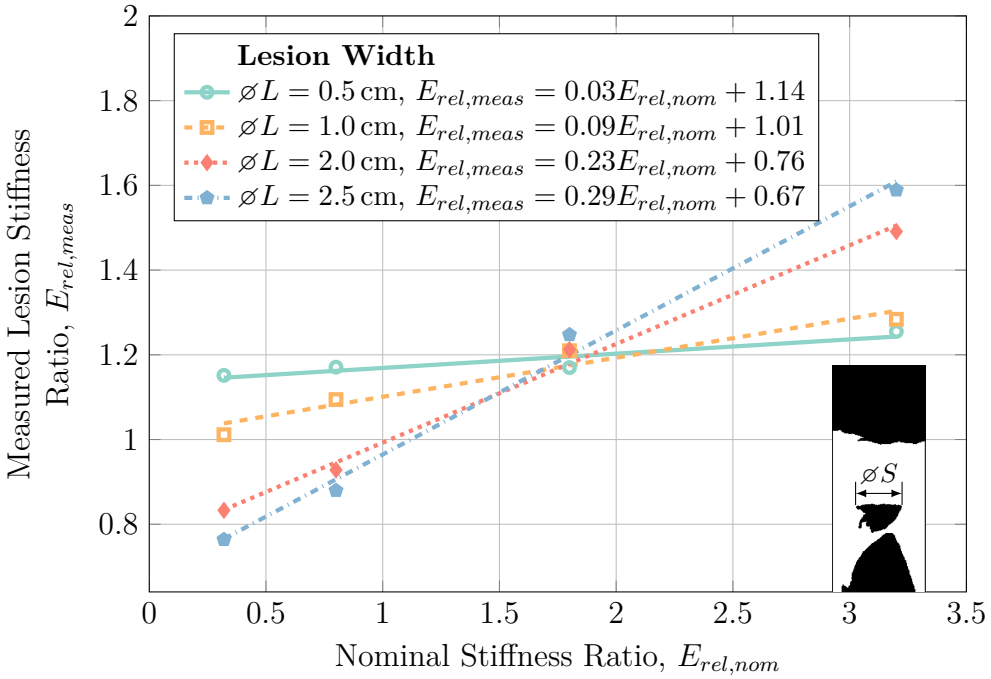

Fig. 3.20: Characterization of lesion width in a Visible Human-MRI model for lesions at a depth of 7.25 cm interrogated with a 4 MHz probing frequency with 5 % applied strain. Small lesions (with a width $\leq$ 1.0 cm) are severely misrepresented and portray general over-estimation of lesion stiffness larger lesions. Lines represent linear regressions of the data.

In Fig. 3.20, it is clear to see than small lesions (with a diameter $\leq$ 1.0 cm) are almost impossible to adequately detect (although larger lesions will be adequately detectable). It is hypothesized that this phenomenon is due to the excessive strain apparent above the boney prominence that is seen in the resultant elastogram given in Fig. 3.21 such that the lesion is "washed out" by the strain field developed by the relatively stiff bone nearby.

In Fig. 3.22, there is little to no dependence of the detection sensitivity

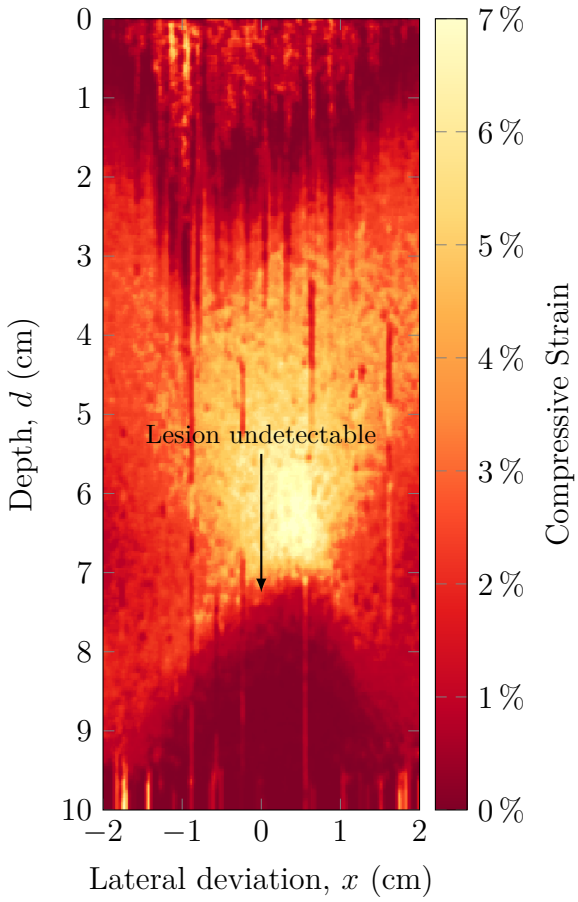

Fig. 3.21: Elastogram for a 0.5 cm wide lesion embedded in the Visible Human-MRI model domain at a depth of 7.25 cm interrogated at 4 MHz with an applied strain of 2.5 %. The lesion is not visible in the resultant elastogram.

on the lesion depth in the Visible Human-MRI model with all depth curves displaying the same profile. However, deeper lesions (lesions closer to the bony prominence) have stiffnesses that are over-estimated with respect to their superficial counterparts. This is hypothesized to be due to the increased strain field present in all of the soft tissue located immediately superior to the bony prominence, but should not pose a serious problem for imaging lesions of this nature.

Numerical values for the characterization plots presented here are given in

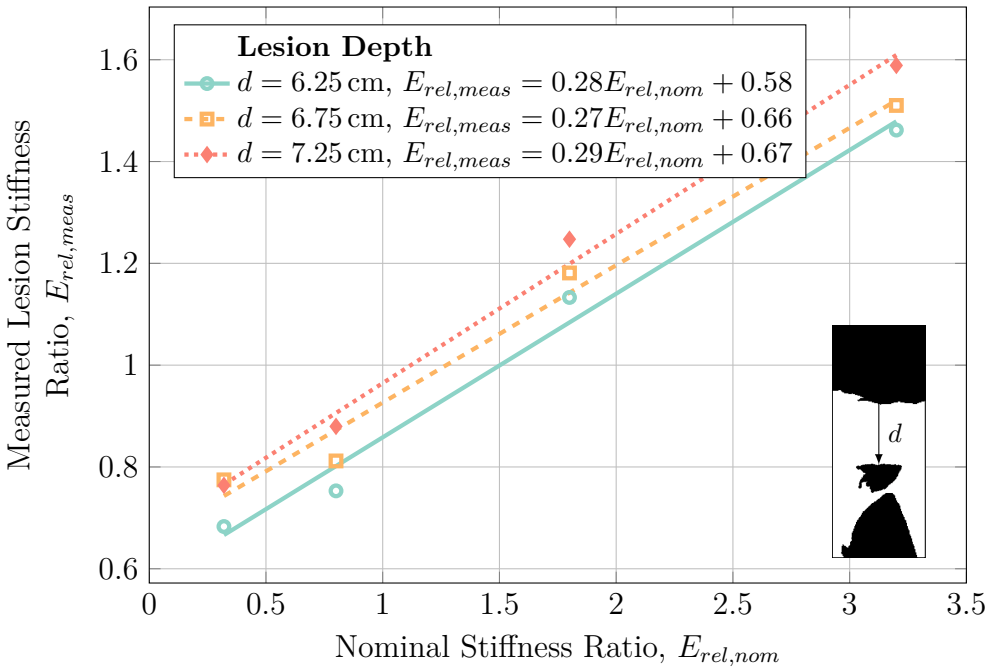

Fig. 3.22: Characterization of lesion depth in a Visible Human-MRI model for lesions with a width of 2.5 cm interrogated with a 4 MHz probing frequency and 5 % applied strain. Deeper lesions (closer to the bony prominence) are have slightly overestimated lesion stiffness ratios as opposed to more superficial lesions while detection sensitivity is not affected by lesion depth. Lines represent linear regressions of the data.

Section A.1 of Appendix A.

3.3.4 Physical Phantom Validation

In order to ensure that the models presented here represented physical realities, a small subset of the cases studied were modelled in a physical phantom, specifically for three lesions with stiffness ratios of 0.56, 1.80, and 3.20 with a diameter of 2.0 cm and at a depth of 3.5 cm, interrogated at 8 MHz with approximately 5 % applied strain. The results of this study are summarized in Fig. 3.23.

As can be seen in Fig. 3.23, a relatively simple (although inexact) rela-

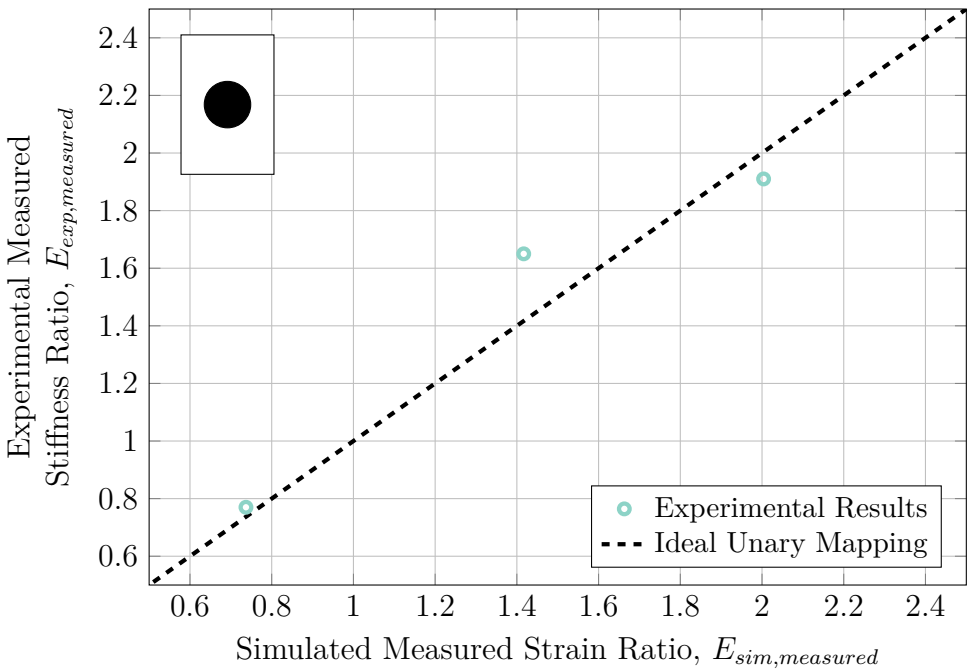

Fig. 3.23: Relation between simulated measured strain ratios and experimental measured strain ratios for a lesion at a depth of 3.5 cm and diameter of 2.0 cm showing general agreement between simulated and experimental cases. Idealization errors are the most likely the cause of the differences seen between simulated and experimental cases.

tionship between simulated and experimental measured strain ratios exists. It must be noted that the finite-element simulations of b-mode image formation and tissue deformation presented here are idealizations of reality and idealization errors such as the ultrasound pulse profile and plane-strain assumption no doubt contributed to the difference seen in Fig. 3.23.

It must be noted that in order to acquire quasi-static elastography results in the physical phantom, the ultrasound transducer was required to be manually manipulated to cause indentation in the phantom, as the technique would most likely be performed in a clinical setting. This was found to be problematic as the ultrasound transducer was difficult to maintain perfectly perpendicular and in-plane during the compression (largely due to the necessity of using coupling